Biorheology 44 (2007) 161–177
IOS Press

Investigation of platelet margination phenomena at elevated shear stress

Rui Zhao [a], Marina V. Kameneva [b,c] and James F. Antaki [a,b,*]
[a] *Department of Biomedical Engineering, Carnegie Mellon University, Pittsburgh, PA, USA*
[b] *Department of Bioengineering, University of Pittsburgh, Pittsburgh, PA, USA*
[c] *McGowan Institute of Regenerative Medicine, University of Pittsburgh, Pittsburgh, PA, USA*

Received 9 October 2006
Accepted in revised form 2 July 2007

Abstract. Thrombosis is a common complication following the surgical implantation of blood contacting artificial organs. Platelet transport, which is an important process of thrombosis and strongly modulated by flow dynamics, has not been investigated under the shear stress level associated with these devices, which may range from tens to several hundred Pascal.

The current research investigated platelet transport within blood under supra-physiological shear stress conditions through a micro flow visualization approach. Images of platelet-sized fluorescent particles in the blood flow were recorded within microchannels (2 cm × 100 μm × 100 μm). The results successfully demonstrated the occurrence of platelet-sized particle margination under shear stresses up to 193 Pa, revealing a platelet near-wall excess up to 8.7 near the wall (within 15 μm) at the highest shear stress. The concentration of red blood cells was found to influence the stream-wise development of platelet margination which was clearly observed in the 20% Ht sample but not the 40% Ht sample. Shear stress had a less dramatic effect on the margination phenomenon than did hematocrit. The results imply that cell–cell collision is an important factor for platelet transport under supra-physiologic shear stress conditions. It is anticipated that these results will contribute to the future design and optimization of artificial organs.

Keywords: Platelet margination, thrombosis, shear stress, artificial organs

1. Introduction

Thrombosis is a common complication following the surgical implantation of blood contacting artificial organs [5,10,14,30,31]. These devices expose blood to both artificial biomaterials and supra-physiological shear rate. Devices featuring small channels, junctions and gaps present particularly difficult challenges due to dimensions that may be of the order of several red blood cells. Figure 1 illustrates two examples: the blade tip of a turbodynamic blood pump and the occluder of a mechanical prosthetic heart valve in which shear stress may traumatize or destroy blood cells [19–21] and/or activate platelets [24]. However, in many circumstances, rather high levels of shear may be sustained by the cells without untoward effects [4,15]. Therefore, the microscopic mechanism governing the dynamics of cell motion through such small gaps at elevated shear rate is not well understood.

The general process of thrombosis includes platelet adhesion on artificial surfaces, which in turn is dependent upon the transport of platelets from the bulk flow to the surface [18,25,29]. Previous research

* Address for correspondence: James F. Antaki, PhD, Department of Biomedical Engineering, Carnegie Mellon University, Pittsburgh, PA 15213, USA. Tel.: 412 802 6431; Fax: 412 802 7813; E-mail: antaki@andrew.cmu.edu

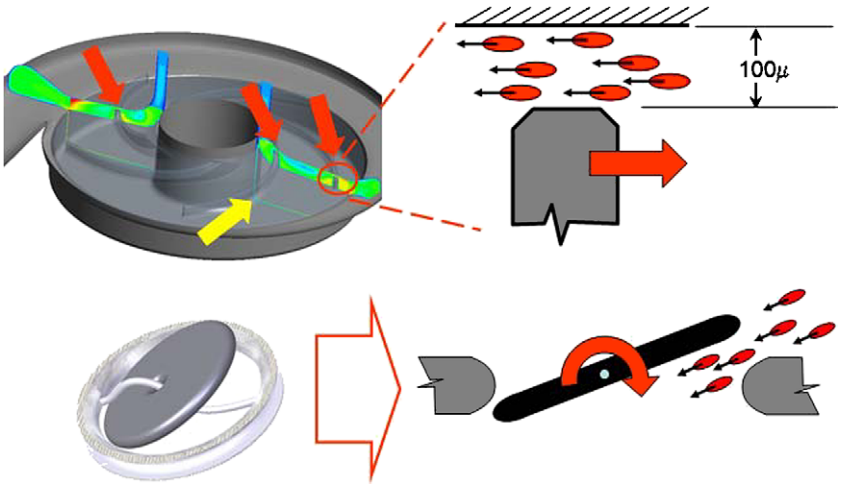

Fig. 1. Examples of artificial devices featuring small blood flow channels with high shear rate. Blade tip gaps of turbodynamic blood pump (red arrows) and bearing journals (yellow arrow) may nominally be on the order of several red blood cells. Mechanical prosthetic heart valves present a similar challenge.

in tube flow under physiologic shear rates showed that platelet transport in blood flow is regulated by both diffusion and convection [9,27], and that platelet diffusivity can be enhanced by the presence of red blood cells (RBCs) [2,27]. The augmented lateral migration of platelets towards the wall in tube flow, *platelet margination*, is believed to result from the complex movement of RBCs, which expel platelets towards the wall as they migrate towards the centerline [9,13,18]. This has been referred to as *exclusion*. An alternate hypothesis is *shear-induced mixing*, where the rotation and random motion of red blood cells in the shear field locally increases platelet diffusivity [1,2].

Extensive experimental studies have been conducted to investigate the effects of various independent parameters on platelet margination, including shear rate, shear stress, hematocrit, the size and concentration of platelets (or platelet-sized particles), and vessel geometry. However, most studies were conducted in the physiological shear stress range, from 0 to about 10 Pa. The extrapolation of these observations to artificial organs, in which shear stress may approach several tens to several hundreds Pascal, has not been conducted.

Therefore, the current study aimed to investigate platelet transport phenomena by micro flow visualization at elevated shear stress approaching 200 Pa. The studies also investigated the influence of hematocrit and the axial development of margination through a sudden constriction. The results were compared with the previous experimental works of Aarts et al. [3] and Eckstein et al. [9], to elucidate the relative influence of elevated shear stress.

2. Materials and methods

2.1. Experimental setup

The experimental setup used for this study is schematically shown in Fig. 2. A suspension of red blood cells and platelet-sized fluorescent particles (described below) was pumped through a rectangular glass microchannel (Vitrocells, VitroCom Inc., Mountain Lakes, NJ) shown in Fig. 3 with dimensions of 2 cm $\times$ 100 μm $\times$ 100 μm. A positive displacement syringe pump (KDS 100, KD Scientific Inc.,

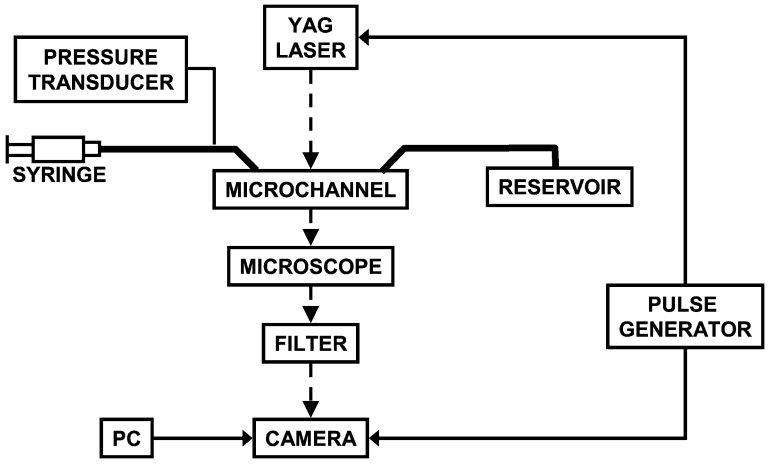

Fig. 2. Schematic of experimental layout for visualization of blood flow within microchannels.

Holliston, MA) provided flow rates of 6 to 15 ml/h – consistent with the prescribed shear stress and duration of exposure. The samples were collected in a small reservoir that was vented to atmospheric pressure. The glass microchannel was bonded to a transparent flow chamber (Fig. 3), which was affixed to the stage of an inverted microscope (IX70, Olympus, Melville, NY) with a 20× objective (LCPlanFL, 20×, NA = 0.40, Olympus, Melville, NY). A CCD camera (PCO Sensicam QE double exposure, The Cooke Corp., Romulus, MI) was attached to the side port of the microscope through a C mount and was used to capture magnified images of platelet-sized fluorescent particles within the microchannel. For most experiments, an Nd:YAG laser (Solo PIV I-15, New Wave Research, Inc., Fremont, CA) with a laser pulse duration of $3 \sim 5$ ns was used to illuminate the blood flow within the channel. An optical notch filter was placed between the microscope and the camera to eliminate the projection of red blood cells. Additional bright field images were obtained using a halogen lamp to visualize the distribution of particles relative to that of the red blood cells.

A series of images (688×520 pixels) was recorded to observe the distribution of the platelet-sized fluorescent particles in the microchannel by synchronizing the laser and the camera using a pulse generator (BK Precision 3011B, Maxtec International Corp., Chicago, IL). The axial location of the microscope stage was recorded by a dial indicator. Images were taken at 6 evenly spaced locations along the length of the channel (see Fig. 3), referenced from the inlet (location 1) to the outlet (location 6).

2.2. Sample preparation

Fresh bovine blood was collected by venipuncture of healthy calves, and was immediately centrifuged at 3000 RPM for 10 minutes. After centrifugation, the plasma and buffy coat, which contained white blood cells and platelets, were removed. Red blood cells (RBC) then were washed three times in phosphate buffered saline (PBS) (P4417, Sigma-Aldrich Corp., St. Louis, MO). Bovine albumin (ICN810133, Fisher Scientific Inc., Fair Lawn, NJ) was added at a concentration of 1% to stabilize cell morphology. The hematocrit of this re-suspension was measured by a micro-centrifuge (Clay Adams TRIAC, Becton, Dickinson and Company, Franklin Lakes, NJ). The suspension was diluted by PBS and further diluted with a mixture of dextrose solution (Dextran 40, Sigma-Aldrich Corp., St. Louis, MO, MW = 37,500) and 0.9% sodium chloride solution (Baxter International Inc., Deerfield, IL) to produce samples with Ht of 20%, 30% and 40%. This latter step allowed us to elevate the viscosity of all samples

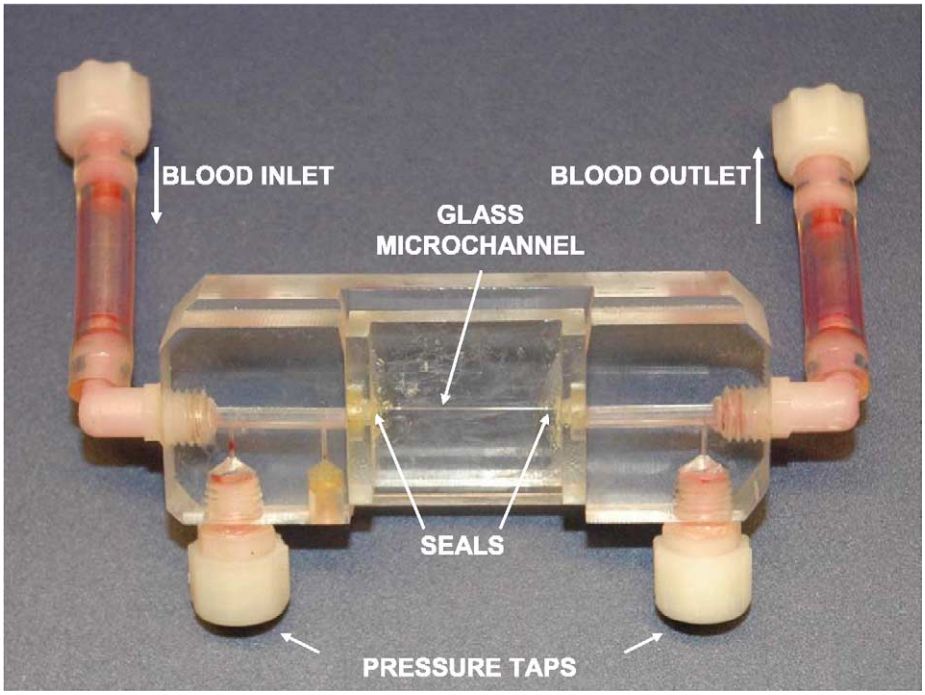

(a)

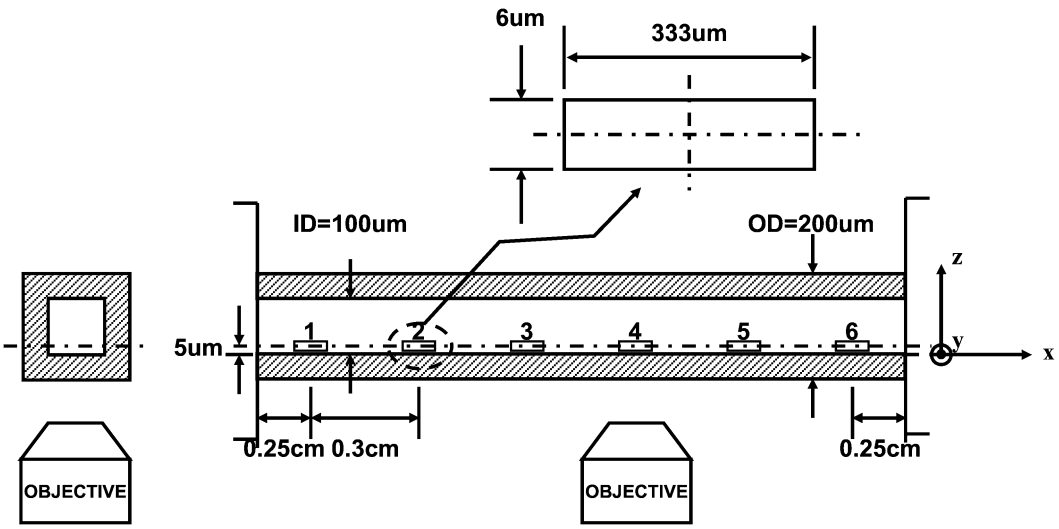

(b)

Fig. 3. (a) Microchannel assembly; (b) Two microchannel side views to show dimensions and the location of regions of interest (not to scale). Local coordinate system is also illustrated. The focal plane is about 5 ± 1 μm in depth from bottom surface of microchannel. Regions of interest: 1 – centered 0.25 cm from entrance; 2–6 – at 0.55, 0.85, 1.15, 1.45 and 1.75 cm, respectively. The objective depth of field is 6 μm according to the product specification.

to a uniform level of 13 ± 2 mPa s irrespective of hematocrit. The viscosity was verified by a cone-and-plate viscometer (Brookfield Digital, Brookfield Engineering Laboratories Inc., Stoughton, MA) at

ambient temperature ($22 \pm 1^{\circ}$C).

A concentrated solution of platelet-sized fluorescent polystyrene particles (R0200, Duke Scientific Corporation, Palo Alto, CA) with a mean diameter of 2 μm, a light excitation peak of 542 nm, emission peak of 612 nm, and concentration of 2.3×10^9/ml was added to the blood suspension in sufficient volume to achieve a bulk concentration of 2.5×10^8/ml, which is within the physiological range of platelet concentration in bovine blood (1×10^8/ml $\sim 4 \times 10^8$/ml). The preparation was mixed for 30 minutes in a plastic centrifuge tube on a rocker plate before the experiments commenced.

2.3. Experimental procedure

Each preparation of blood was infused at incrementally increasing flow rates by the syringe pump, corresponding to the shear stress levels in Table 1. The entire flow path was purged with 0.9% sodium chloride solution between blood samples.

Images were acquired at a series of locations along the flow path from 0.25 cm distal to the channel inlet to 0.25 cm proximal to the channel outlet. The microscope was focused on an image plane nominally 5 ± 1 μm above the bottom surface of the channel (see Fig. 3). Depth was measured by the scale on the fine focus adjustment. Backlash errors were avoided by moving the stage in a single direction, from bottom to top. Based on a depth of field of 6 μm, the volume of interest consisted of a rectangular prism (333 μm length × 100 μm width × 6 μm depth) directly adjacent to the bottom (proximal) interior wall of the channel. The axial distance between two successive locations was 0.3 cm, measured by a dial indicator attached to the microscope stage. For each region of interest, 100 images were recorded by digital camera to the PC. The frame rate (sampling rate) was controlled by the pulse generator ($\leqslant$4 Hz) to assure complete replacement of the cell population in each sample.

2.4. Image analysis

Images were processed with a custom-designed Matlab program (Mathworks, Natick, MA) to obtain the concentration profile of platelet-sized particles (Fig. 4). First, the images were cropped to isolate the flow region of the microchannel. Subsequent processing entailed background homogenization to equilibrate uneven illumination and contrast-enhancement by histogram stretching. The minimal and maximal intensity values in this process were carefully selected according to the original intensity histogram. The particles in the image were identified by thresholding followed by erosion to eliminate spurious noise. The threshold was adjusted to minimize the error between manually and automatically counted particles. This process was repeated for five random frames and the same threshold was used thereafter. Manual count was performed by the same expert in all experiments. Figure 5(a) shows the final processed image compared to the raw image.

Table 1

The flow rate and shear exposure inside the microchannel for the experimental conditions studied. The shear stresses under varied flow rates were calculated theoretically. Exposure time was defined as the duration of a cell passing through the microchannel and was determined by dividing the length of the microchannel by the average flow velocity. Laser pulse duration is the laser beam flashing time while taking one image frame and is in the order of nano seconds

Condition	Flow rate (ml/h)	Shear stress (Pa)	Exposure time (ms)	Laser pulse duration (ns)
Low	3	38	240	$3 \sim 5$
Medium	9	114	80	$3 \sim 5$
High	15	193	48	$3 \sim 5$

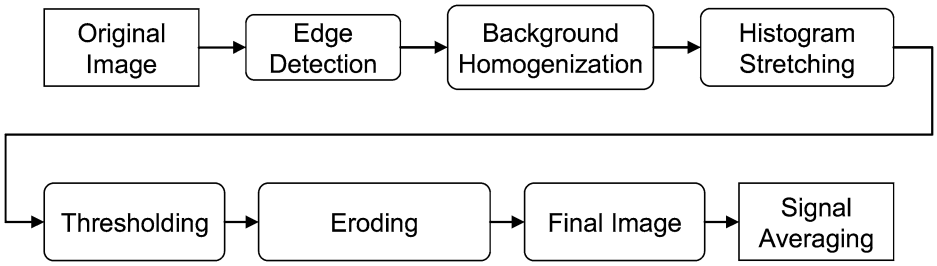

Fig. 4. Image processing procedure.

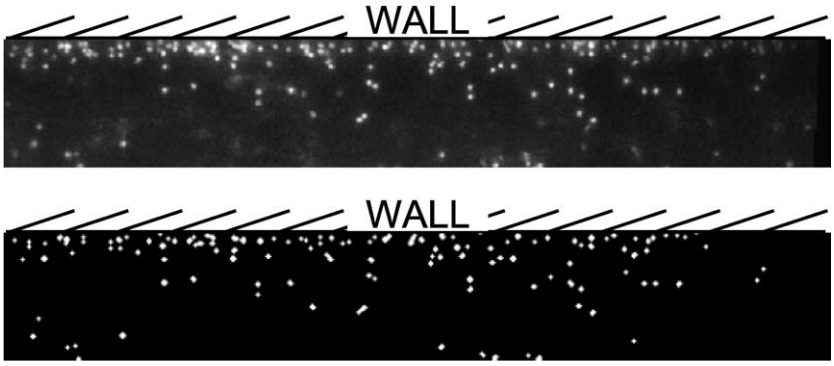

(a)

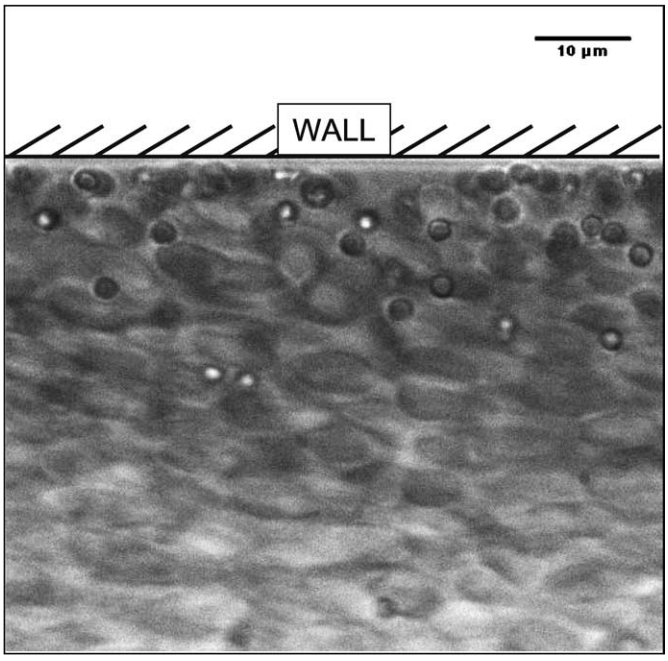

(b)

Fig. 5. Sample images of half-width of channel. (a) Top: raw cropped image; Bottom: processed image; (b) Bright field image showing platelet-sized particle margination and red blood cell deformation (half channel, 100× objective, Ht = 40%, $Q = 6$ ml/h, maximum shear stress = 76 Pa).

The concentration profile of particles was obtained by first partitioning the image into specified number of lateral bands (=20, 40 and 80). The coarse banding ($n = 20$) was evenly distributed, corresponding to a width of 5 μm. The fine density banding ($n = 80$) was concentrated near the wall, corresponding to 1 μm within 20 μm of the wall, and 1.5 μm in the core. The corresponding band-width for medium density banding was 2 μm and 3 μm, near the wall and in the core, respectively. The number of particles in each band was counted by a custom-written Matlab program and averaged over 100 images. The concentration profile of the platelet-sized particles was then normalized as

$$C(r) = \frac{(\#\text{ particles in RoI})/(\text{total volume of RoI})}{(\text{bulk particle count}/\text{unit volume})}, \tag{1}$$

where $C(r)$ refers to the relative concentration. The volume associated with the region of interest (RoI) was estimated based on the depth of field specifications of the objective (=6 μm).

2.5. Statistical method

Student's t-test was used to evaluate differences between the observed particle concentrations. A value of $p < 0.05$ was assumed to indicate statistical significance.

2.6. Stress field analysis

Theoretical velocity profiles were obtained using the closed form solution of Navier–Stokes equation for a fully developed flow in a rectangular duct [28]. Assuming blood to be an incompressible Newtonian fluid:

$$u(y,z) = \frac{16a^2}{\mu\pi^3}\left(-\frac{\mathrm{d}p}{\mathrm{d}x}\right)\sum_{i=1,3,5,\ldots}^{\infty}(-1)^{(i-2)/2}\left[1-\frac{\cosh(i\pi z/2a)}{\cosh(i\pi/2)}\right]\times\frac{\cos(i\pi y/2a)}{i^3}, \tag{2}$$

where the pressure gradient was calculated from the given flow rate:

$$\left(-\frac{\mathrm{d}p}{\mathrm{d}x}\right) = 3\mu Q\Big/\left(4a^4\left[1-\frac{192}{\pi^5}\sum_{i=1,3,5,\ldots}^{\infty}\frac{\tanh(i\pi/2)}{i^5}\right]\right), \tag{3}$$

where a is half of the channel width (for square channel); u is velocity; μ is the sample viscosity; p is pressure; and Q is flow rate.

The scalar shear stress was calculated as

$$|\underline{\underline{\sigma}}| = 2\mu|\underline{\underline{E}}| = \mu\sqrt{\left(\frac{\partial u_x}{\partial y}+\frac{\partial u_y}{\partial x}\right)^2+\left(\frac{\partial u_z}{\partial y}+\frac{\partial u_y}{\partial z}\right)^2+\left(\frac{\partial u_x}{\partial z}+\frac{\partial u_z}{\partial x}\right)^2}, \tag{4}$$

where $|\underline{\underline{E}}|$ is the norm of the rate of strain tensor $\underline{\underline{E}}$.

Assuming unidirectional flow, the equation is simplified to

$$|\underline{\underline{\sigma}}| = \mu\sqrt{\left(\frac{\partial u_x}{\partial y}\right)^2+\left(\frac{\partial u_x}{\partial z}\right)^2}. \tag{5}$$

3. Results

3.1. Hydrodynamics

The relationship between pressure and flow rate in the microchannel was found to be highly linear ($R^2 = 0.98$). Likewise, the measured pressure agreed well with the pressure predicted from Eq. (3) (see Fig. 6). This suggests that the influence of the entrance and diffuser of the channel was negligible. Figure 7 shows the computation of shear stress distribution by Eq. (5) on the horizontal plane 5 μm above the bottom face at the maximum flow rate of 15 ml/h. Under these conditions, the near-wall shear stress is 193 Pa. The corresponding average transit time (exposure) of cells through the glass microchannel, determined by dividing the length of the microchannel by the average axial velocity, is 48 ms. Table 1 summarizes these results.

3.2. Effect of partition band resolution on shape of concentration profile

Figure 8 illustrates the concentration profiles of a 20% hematocrit sample at a flow rate of 15 ml/h according to the three different partition densities described above. For clarity, the figure is derived from a mirror image of half-width measurements. All three methods revealed a radial increase of particle concentration from the centerline towards the wall. The fine partitioning (1 μm wall and 1.5 μm core) however, revealed a small depletion in the layer nearest the wall (within approximately 1 μm), hence

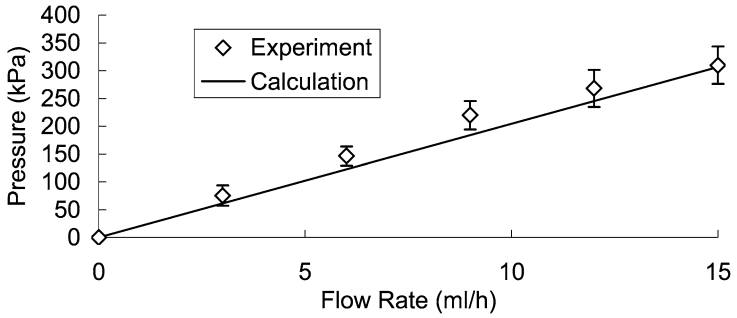

Fig. 6. Pressure–flow rate relationship. The relationship between pressure and flow rate was highly linear ($R^2 = 0.98$). The measured pressure was in good agreement with the theoretically predicted pressure, which suggests that the influence of entrance and diffusion effects in the channel were negligible. The pressure reached 306 kPa at the flow rate of 15 ml/h.

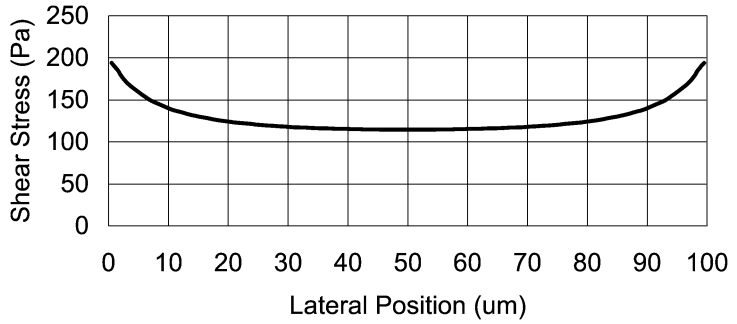

Fig. 7. Shear stress distribution. The shear stress was computed from Eq. (5) on the horizontal plane 5 μm above the bottom face at the maximum flow rate of 15 ml/h. Under these conditions, the near-wall shear stress was 193 Pa.

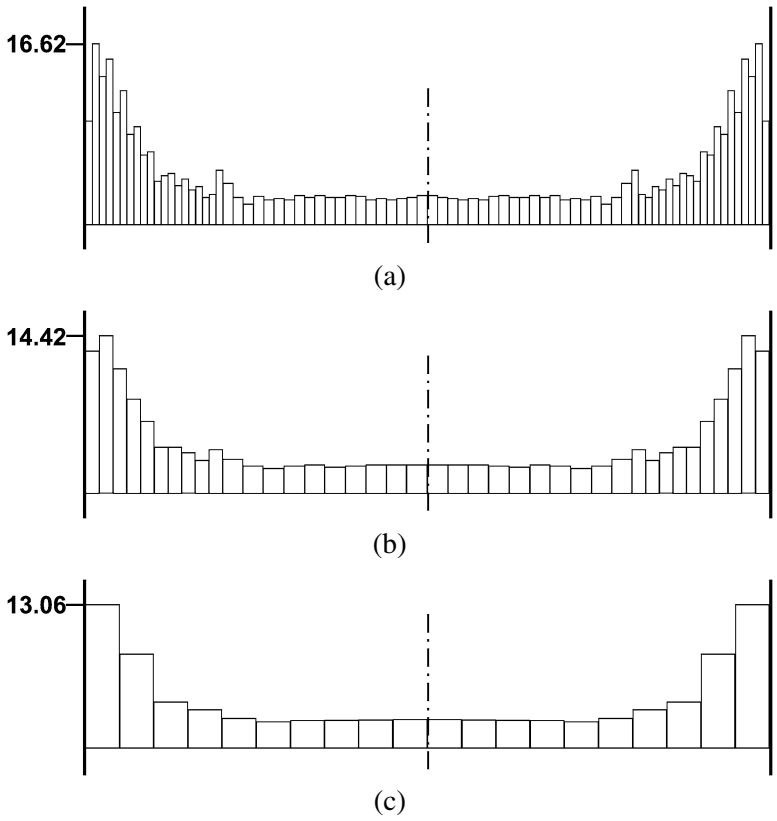

Fig. 8. Concentration profile of platelet-sized particles in glass microchannel (hematocrit = 20%, Q = 15 ml/h, maximum shear stress = 193 Pa, outlet). (a) The fine density banding (n = 80) was concentrated near the wall, corresponding to 1 μm within 20 μm of the wall and 1.5 μm in the core; (b) The medium density banding (n = 40) was also concentrated near the wall, corresponding to 2 μm within 20 μm of the wall and 3 μm in the core; (c) The coarse banding (n = 20) was evenly distributed, corresponding to a width of 5 μm. (Full-width profile, shown for clarity is derived from mirror-image of half-width data.)

demonstrating a unimodal distribution with a peak approximately 2 μm from the wall. This feature was not observed with the coarse partitioning (see Fig. 8(c)). Based on this analysis, we used the fine partition method (Fig. 8(a)) to construct the concentration profile and calculate the particle near-wall excess (PNWE) of all subsequent experiments. The coarse partition (Fig. 8(c)), which better represented the average near-wall concentration (and hence less prone to noise), was used to compare the margination magnitude under different experimental conditions (e.g. to investigate the axial development of margination).

These concentration profiles are comparable to those provided by Aarts et al. [3] and Eckstein et al. [9]. Aarts presented a monotonically increasing concentration from centerline to the wall, corresponding to the coarse partitioning in the current experiment. By contrast, Eckstein et al. [9] presented an unimodal profile, with its peak approximately 2 μm away from the tube wall, similar to the current results for fine partitioning (see Fig. 9).

3.3. Development of axial margination

The particle concentration profiles at three axial locations (position 1, 4 and 6) for samples of 20% and 40% hematocrit at a flow rate of 15 ml/h are shown in Fig. 10 (as in Fig. 8, a full-width illustration

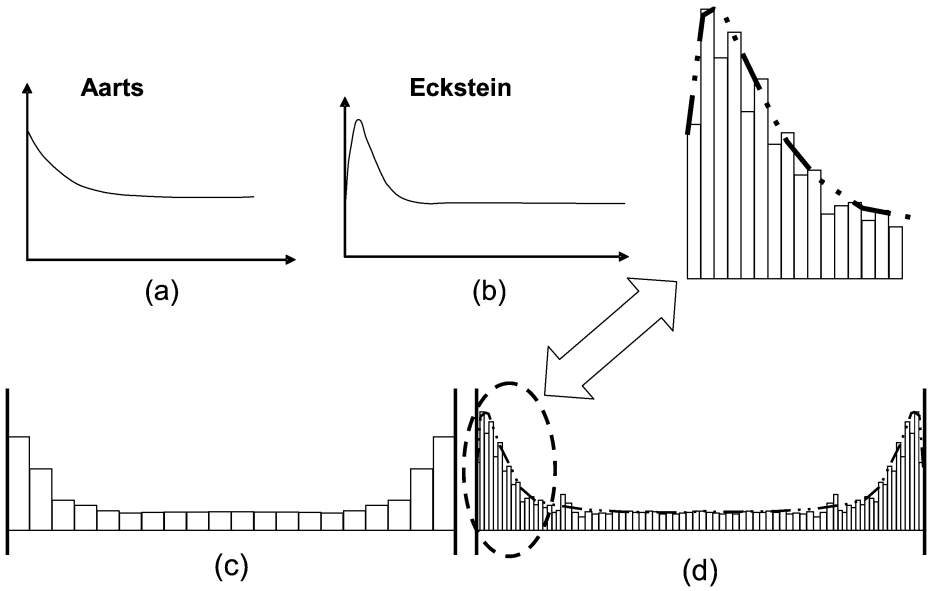

Fig. 9. Concentration profile of particles (a) Aarts' model [3]; (b) Eckstein's model [9]; both (a) and (b) are from the curve fitting using the data of Xu et al. [29]. (c) Concentration profile with partition band width of 5 μm, hematocrit = 20%, flow rate = 15 ml/h, maximum shear stress = 193 Pa, near outlet; (d) concentration profile with partition band width of 1 μm in the 20 μm near-wall regions and 1.5 μm in other regions, hematocrit = 20%, flow rate = 15 ml/h, maximum shear stress = 193 Pa, near outlet. When resolved to 1 μm thick sub-regions, the current experimental observations most closely correspond to the unimodal profile of Eckstein et al. However, when coarsened to a width of 5 μm it is not possible to spatially resolve this feature, and the profile appears to be monotonic.

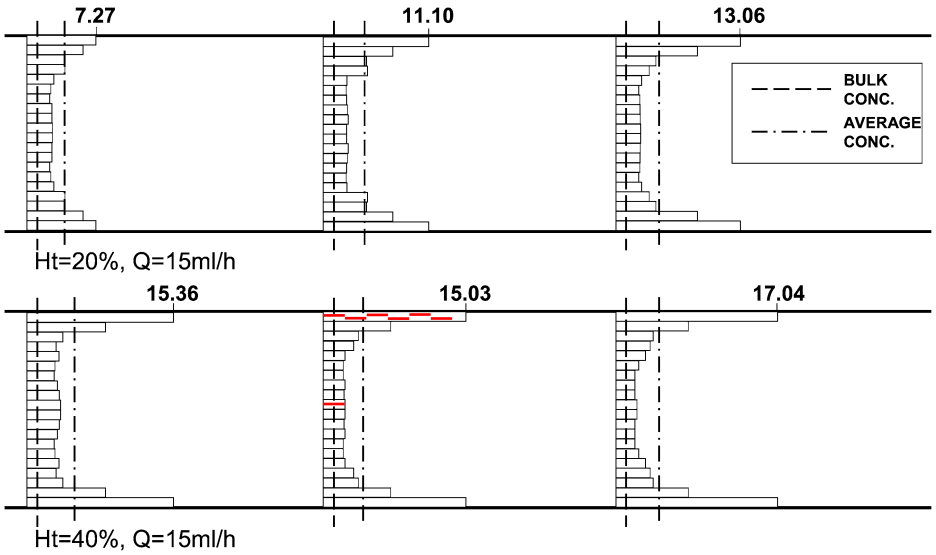

Fig. 10. Axial development of concentration boundary layer, Q = 15 ml/h, maximum shear stress = 193 Pa, band width = 5 μm. Only positions 1, 4 and 6 are shown. Axial boundary layer development was observed in the sample with hematocrit of 20% (top). The near-wall relative concentration of platelet-sized particles increases from 7.27 near inlet to 13.06 near outlet. The 40% Ht sample demonstrates almost instantaneous boundary layer development. The terminal near-wall concentration (at the outlet) is greater for the 40% Ht sample as compared to the 20% sample. (Full-width concentration profile illustrated based on mirror image of half-width measurements.)

is depicted based on a mirror image of half-width data). The axial development of the margination layer was clearly observed in the sample with a hematocrit of 20%. The near-wall concentration increased from 7.27 near the inlet (position 1) to 13.06 near the outlet (position 6). There was no such development observed in the 40% Ht sample in which the concentration profile was established almost instantly.

The figure also indicates reference values for the average concentration within the image and the bulk concentration of the sample. Compared to the bulk, the average concentration within the focal plane, which is 5 μm above the bottom surface, was 3.68 to 4.96 times greater. The relative concentration near the centerline was also approximately 1 to 2 times greater than the bulk concentration. Therefore, these results indicated the occurrence of platelet margination in the z (depth) direction.

3.4. Particle excess at the wall

To quantify the accumulation of particles near the wall, a particle near-wall excess (PNWE) index was defined as:

$$\text{PNWE} = \int_0^{15\ \mu\text{m}} C(r)\,\mathrm{d}r/(\ \#\ \text{of partition bands}), \tag{6}$$

where $C(r)$ is the relative particle concentration as a function of radial position. This integral was computed by the trapezoidal method using the particle concentration in the sub-regions within a distance of 15 μm from the microchannel wall, based on fine partitioning. The choice of 15 μm distance was based on the observation of the concentration gradient shown in Fig. 11, which illustrates a toe transition in this range. The integral was normalized to the number of partition bands to eliminate the effect of band resolution. Table 2 summarizes the results of these studies in terms of PNWE. Although all cases exhibited near-wall excess, the 40% Ht sample demonstrated significantly greater PNWE ($p < 0.05$) than the 20% Ht sample at the channel inlet for all flow rates (Fig. 12(a)). However, there was no statistical difference observed at the outlet between samples for either flow rate (Fig. 12(b)). The PNWE also increased from

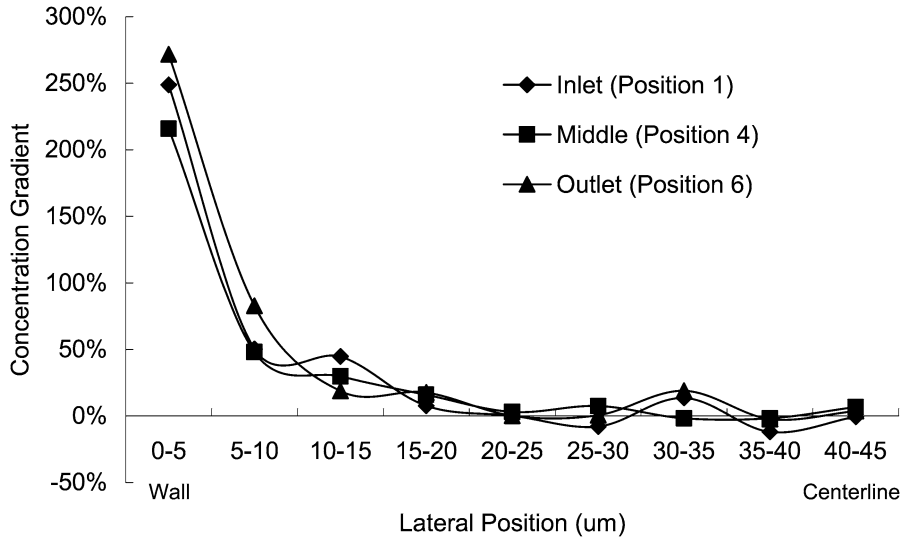

Fig. 11. Concentration gradient in the lateral direction (hematocrit = 40%, Q = 3 ml/h, maximum shear stress = 38 Pa) for half-width of channel. Toe of the curve defined at 15 μm from the wall. Data averaged over 300 frames.

Table 2

Platelet near-wall excess (PNWE) at axial positions 1, 4 and 6, at three flow rates (3 $\sim$ 15 ml/h). The PNWE increased from inlet (5.47 ± 0.15) to outlet (7.71 ± 0.39) for 20% hematocrit samples remained more constant for 40% hematocrit samples (7.70 ± 0.83 vs. 8.11 ± 0.54)

	Ht = 20%			Ht = 40%		
	$Q = 3$ ml/h	$Q = 9$ ml/h	$Q = 15$ ml/h	$Q = 3$ ml/h	$Q = 9$ ml/h	$Q = 15$ ml/h
Position 1	5.32	5.62	5.46	7.06	7.42	8.62
Position 4	6.50	7.07	7.11	7.46	7.71	8.14
Position 6	7.42	7.57	8.15	7.85	7.74	8.74

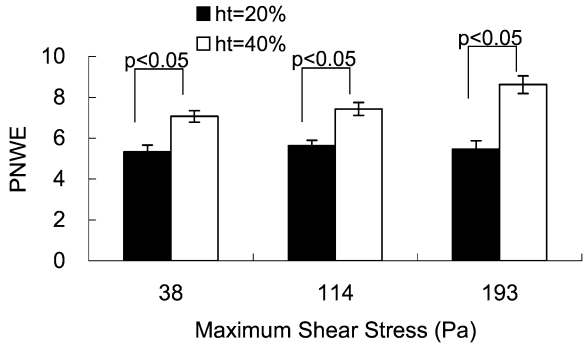

(a)

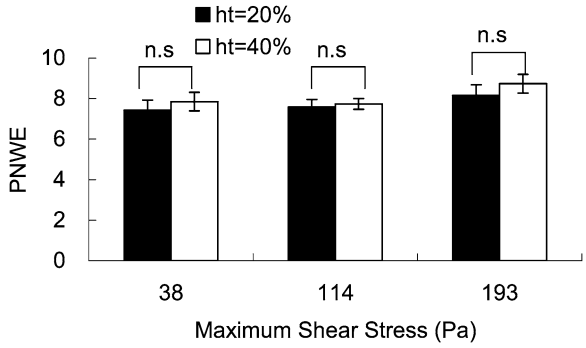

(b)

Fig. 12. Platelet near-wall excess (PNWE) with 95% confidence interval. Particle near-wall excess was defined as the integral of the particle relative concentration in the sub-regions within a distance of 15 μm from the microchannel wall divided by the number of sub-regions. (a) At inlet: PNWE for sample with hematocrit of 20% is lower than the one for sample with hematocrit of 40% at all flow rates ($p < 0.05$); (b) PNWE at outlet: no statistically significant dependence on hematocrit at all flow rates. All results are shown for viscosity = 13 mPa s.

the inlet (5.47 ± 0.15) to outlet (7.71 ± 0.39) for 20% Ht samples, but remained relatively constant for 40% Ht samples (7.70 ± 0.83 vs. 8.11 ± 0.54).

3.5. The effect of dextrose solution on margination

The preceding experiments used a solution of dextrose (Dextran 40) to augment the shear stress at nominal flow rates. Therefore, there is a possibility that Dextran itself may be responsible for the margination phenomenon. Thus, an independent study was conducted comparing margination of a blood

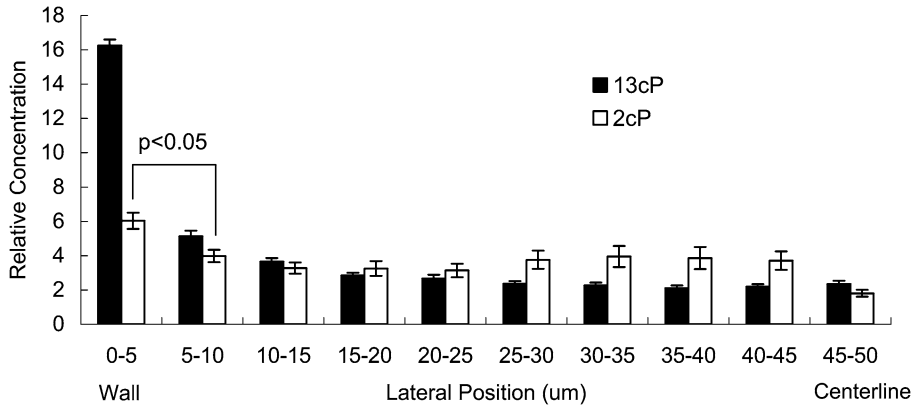

Fig. 13. Platelet-sized particle lateral distribution at different viscosity, hematocrit = 40%, outlet. The maximal shear rate was 14850/s. $\mu = 2$ mPa s, sample without Dextran; $\mu = 13$ mPa s, sample with Dextran. Platelet margination phenomenon was observed in the sample without Dextran ($\mu = 2$ mPa s) ($p < 0.05$). The near-wall concentration in the lower viscosity sample is around 2.67 times lower than that in the higher viscosity sample, to which Dextran 40 was added.

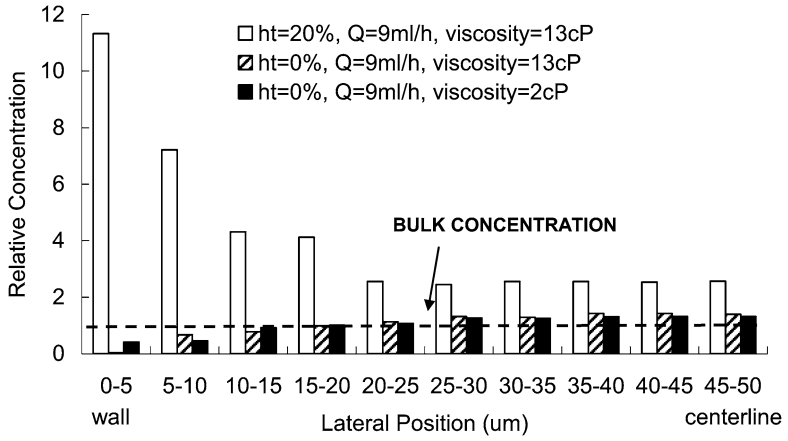

Fig. 14. Platelet-sized particle lateral distribution with and without RBCs, $Q = 9$ ml/h, maximum shear stress = 114 Pa, outlet. There is no particle margination in the sample without RBCs.

sample without Dextran to a sample prepared with Dextran at similar shear rates (see Fig. 13). The respective dynamic viscosities of these samples were 2 and 13 mPa s. The hematocrit and maximum shear rate of both samples was 40% and 14850/s, respectively.

Images were acquired near the microchannel outlet to ensure a fully developed boundary layer. The particle distribution of the unmodified sample demonstrated a near-wall excess profile similar to that of the Dextran-modified sample. Thus, although the presence of Dextran is not required to induce margination, Fig. 13 shows that the magnitude of the near-wall concentration was much lower without Dextran, being reduced by 267%, from 16.3 to 6.1 ($p < 0.05$). It should be noted, however, that the magnitude of the shear stress was reduced by 650% in the absence of Dextran. It is therefore necessary compare the effects of RBC to that of Dextran to quantify margination in vivo. This is shown in Fig. 14 that illustrates the relative influence of RBC compared to Dextran. It can be seen that Dextran by itself does not cause any lateral variation in cell-free suspension of particles. By contrast, the presence of RBCs (20% Ht) illustrates their essential role in platelet margination.

4. Discussion

The phenomenon of platelet margination in blood vessels has been known for many years [9,13,18]. Under physiologic conditions, it is understood to promote hemostasis by concentrating platelets near the wall where they are most needed in case of injury. The hemodynamics of prosthetic devices, however, may exhibit elevated shear rates near the wall sufficient to activate platelets. In turn, the maintenance of a platelet-rich layer near the surface would promote undesirable thrombosis. However neither the characteristics nor existence of this phenomenon at elevated shear stress has previously been reported.

The current studies successfully confirmed the existence of platelet margination for shear stress up to 193 Pa. Furthermore, a profound hematocrit effect was found on the development of the boundary layer, implying that cell–cell collisions are an important factor for platelet transport under supra-physiologic shear stress conditions. The effect of shear stress was found to be not as dramatic as hematocrit over the current range of shear stresses.

One may speculate that the narrow gap of a prosthetic valve or impeller blade may not have sufficient length for a margination layer to be established. However, micro flow visualization of blood seeded with platelet-sized fluorescent particles revealed nearly instantaneous margination under certain conditions. The current results illustrated the importance of hematocrit upon the lateral convection of platelets as previously reported by Eckstein et al. [6,8,22,26]. Furthermore, the concentration profile at high shear was found to resemble these latter observations. When re-sampled at coarser spatial density, the data could also be compared to the monotonic relationship observed by Aarts et al. [3]. The disparity between these two results might be attributed to differences in vessel diameter (3 mm vs. $\leqslant$220 μm) or due to the difference in spatial resolution which was approximately 3 μm in the studies of Eckstein et al. [6] versus 50 μm reported by Aarts et al. [3]. Because of the coarse resolution of the measurements of Aarts et al., the characteristic shape of platelet lateral concentration in larger channels has yet to be confirmed. However, one may hypothesize that since the Fahraeus–Lindqvist effect is known to be influenced by vessel diameter [11], it is possible that the concentration profile of platelets in microvessels also differs from large vessels. This is a topic for future study.

Since the microchannel cross-section is square, one would expect margination to occur around the entire periphery. Hence, the distribution of cells and particles observed in the lateral direction should also occur in the perpendicular direction (z-direction), parallel to the microscope objective. This was indeed confirmed by observing that the average concentration within the focal plane near the centerline was much greater than the bulk concentration.

The profound effect of hematocrit on the lateral distribution of particles supports the hypotheses that collisions between RBC and platelets [9,13,18] are responsible for the enhanced radial advection. There was no margination observed in the samples with zero hematocrit. This result concurs with Eckstein et al., who found that a critical level of 7% Ht under physiological shear stress was necessary for margination to be observed [26]. These experiments could not confirm nor refute whether cell rotation had any effect on platelet diffusivity, as postulated previously [2,27]. However, Goldsmith et al. [12] demonstrated that cell crowding due to increased hematocrit prevents cellular rotation. This suggests that rotation is not a likely contributor to the margination observed in the higher hematocrit samples.

Compared to the effect of hematocrit, the effect of shear stress within the range 38–193 Pa was much less dramatic. A possible reason could be that the RBCs rapidly reach an elongation plateau under this range of shear stress. In a previous in-vitro study, we observed such a plateau at approximately 60 Pa [32]. This would imply that the shape of the RBCs is also an important factor in the margination phenomenon.

The current experiments employed Dextran with a molecular weight of 40,000 Dalton to increase the viscosity of the suspension. Although the occurrence of the margination phenomenon was shown to be independent of the presence of Dextran, the near-wall excess was amplified by Dextran. This could be explained by the increase of shear stress and/or possibly a chemically induced aggregation of RBCs by Dextran. The phenomenon of Dextran-induced aggregation has been observed by previous researchers [7,16,17,23]. However, we did not find aggregation of bovine RBCs under the current experimental conditions (see Figs 5(b) and 15). It is unlikely that RBC aggregation could cause the observed increase in small particle margination. Therefore, there are other mechanisms which produce this phenomenon that need additional investigation. A previous study by Eckstein et al. had also observed an increase in margination with increasing Dextran concentration [8]. They reported a nonlinear, asymptotic relationship between near-wall excess and shear stress. This would explain the disproportionately smaller increase in near-wall excess (267%) to that of shear stress (650%).

The error introduced by the automatic image processing was evaluated by randomly selecting 5 images in each experimental setting and comparing the difference between automatic and manual particle counts. The error was minimized within 10% by tuning the image processing parameters. Since this is a subjective measure, it may introduce a source of systematic error.

A related source of error is the discrimination of particles out of the focal plane. These unfocused particles may be erroneously counted either manually or automatically. This could result in overestimation of concentration. This may explain why the relative concentration near the centerline in Fig. 14 was slightly higher than the bulk concentration for the sample without RBCs. However, these artifacts were reduced in the sample with RBCs, which blocked most unfocused particles. This source of systematic error should not affect the primary conclusions of this study.

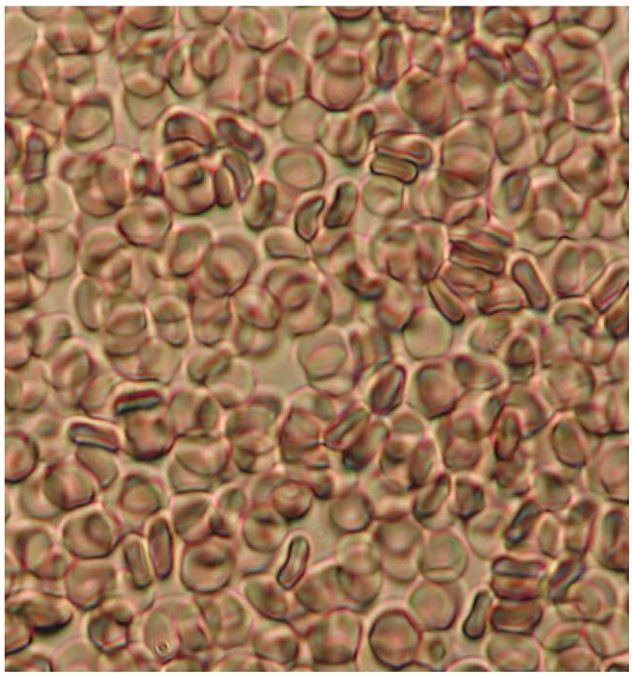

Fig. 15. Phase contrast microscopy image of RBCs in Dextran 40 solution. Hematocrit = 40%. There is no RBC aggregation observed.

Also, the relative size of the particles (2 μm) to the depth of field (6 μm) may result in overlapping particles, which the image processing program is incapable of identifying. This may play a role in the reduced near-wall platelet concentration. More sophisticated automatic counting methods are being sought to eliminate this error in the future.

Additional experimental errors of the current investigation may have been introduced by the relatively shallow depth of the focal plane, which was 5 μm ($\pm$1 μm) above the bottom face. The opacity of RBCs in the solution obstructed viewing deeper levels of the particle distribution. This limitation could be addressed in a future study by using RBC ghost cells.

There is clearly much opportunity to further the understanding of microscopic behavior in the complex flow of blood cells. Additional experiments will be essential for developing improved multi-phase, multi-scale models of hemorheology.

References

[1] P.A. Aarts, P.A. Bolhuis, K.S. Sakariassen, R.M. Heethaar and J.J. Sixma, Red blood cell size is important for adherence of blood platelets to artery subendothelium, *Blood* **62** (1983), 214–217.
[2] P.A. Aarts, R.M. Heethaar and J.J. Sixma, Red blood cell deformability influences platelets–vessel wall interaction in flowing blood, *Blood* **64** (1984), 1228–1233.
[3] P.A. Aarts, S.A. van den Broek, G.W. Prins, G.D. Kuiken, J.J. Sixma and R.M. Heethaar, Blood platelets are concentrated near the wall and red blood cells, in the center in flowing blood, *Arteriosclerosis* **8** (1988), 819–824.
[4] J.F. Antaki, K.C. Butler, R.L. Kormos, A. Kawai, H. Konishi, J.P. Kerrigan, H.S. Borovetz, T.R. Maher, M.V. Kameneva and B.P. Griffith, In vivo evaluation of the Nimbus axial flow ventricular assist system. Criteria and methods, *ASAIO J.* **39** (1993), M231–M236.
[5] S. Arslan, F. Gundogdu and E. Bozkurt, Images in cardiology. Permanent pacemaker lead thrombosis leading to recurrent pulmonary embolism, *Heart* **92** (2006), 597.
[6] D.L. Bilsker, C.M. Waters, J.S. Kippenhan and E.C. Eckstein, A freeze-capture method for the study of platelet-sized particle distributions, *Biorheology* **26** (1989), 1031–1040.
[7] D.E. Brooks, The effect of neutral polymers on the electrokinetic potential of cells and other charged particles. IV. Electrostatic effects in dextran-mediated cellular interactions, *J. Colloid Interface Sci*. **43** (1973), 714–726.
[8] E.C. Eckstein, A.W. Tilles and F.J. Millero 3rd, Conditions for the occurrence of large near-wall excesses of small particles during blood flow, *Microvasc. Res*. **36** (1988), 31–39.
[9] E.C. Eckstein and F. Belgacem, Model of platelet transport in flowing blood with drift and diffusion terms, *Biophys. J*. **60** (1991), 53–69.
[10] D. Fabijanic, L. Giunio, M. Vujicic, I. Vukovic, R. Ermacora and N. Knezevic, Right atrial pacemaker lead thrombosis incidentally detected by transesophageal echocardiography, *Coll. Antropol*. **29** (2005), 159–161.
[11] R. Fåhraeus and T. Lindqvist, Viscosity of blood in narrow capillary tubes, *Am. J. Physiol*. **96** (1931), 562–568.
[12] H.L. Goldsmith and J.C. Marlow, Flow behavior of erythrocytes. II. Particle motions in concentrated suspensions of ghost cells, *J. Colloid Interface Sci*. **71** (1979), 383–407.
[13] H.L. Goldsmith and V.T. Turitto, Rheological aspects of thrombosis and haemostasis: basic principles and applications. ICTH-Report – Subcommittee on Rheology of the International Committee on Thrombosis and Haemostasis, *Thromb. Haemostasis* **55** (1986), 415–435.
[14] D.J. Goldstein, Coagulation and thrombotic complications associated with ventricular assist devices, *Clin. Adv. Hematol. Oncol*. **3** (2005), 766–768.
[15] N.L. James, A.L. van der Meer, G.A. Edwards, S.R. Snelling, J.D. Begg, D.S. Esmore and J.C. Woodard, Implantation of the VentrAssist implantable rotary blood pump in sheep, *ASAIO J*. **49** (2003), 454–458.
[16] K.M. Jan and S. Chien, Influence of the ionic composition of fluid medium on red cell aggregation, *J. Gen. Physiol*. **61** (1973), 655–668.
[17] K.M. Jan and S. Chien, Role of surface electric charge in red blood cell interactions, *J. Gen. Physiol*. **61** (1973), 638–654.
[18] A. Jordan, T. David, S. Homer-Vanniasinkam, A. Graham and P. Walker, The effects of margination and red cell augmented platelet diffusivity on platelet adhesion in complex flow, *Biorheology* **41** (2004), 641–653.
[19] M.V. Kameneva, A. Undar, J.F. Antaki, M.J. Watach, J.H. Calhoon and H.S. Borovetz, Decrease in red blood cell deformability caused by hypothermia, hemodilution, and mechanical stress: factors related to cardiopulmonary bypass, *ASAIO J*. **45** (1999), 307–310.

[20] M.V. Kameneva, P.F. Marad, J.M. Brugger, B.M. Repko, J.H. Wang, J. Moran and H.S. Borovetz, In vitro evaluation of hemolysis and sublethal blood trauma in a novel subcutaneous vascular access system for hemodialysis, *ASAIO J*. **48** (2002), 34–38.
[21] M.V. Kameneva, G.W. Burgreen, K. Kono, B. Repko, J.F. Antaki and M. Umezu, Effects of turbulent stresses upon mechanical hemolysis: experimental and computational analysis, *ASAIO J*. **50** (2004), 418–423.
[22] J.F. Koleski and E.C. Eckstein, Near wall concentration profiles of 1.0 and 2.5 microns beads during flow of blood suspensions, *ASAIO Trans*. **37** (1991), 9–12.
[23] S. Shin, Y. Ku, J.S. Suh, S.Y. Moon and J.Y. Jang, Characteristics of blood flow resistance under transverse vibration: red blood cell suspension in Dextran-40, *Ann. Biomed. Eng*. **31** (2003), 1077–1083.
[24] T.A. Snyder, M.J. Watach, K.N. Litwak and W.R. Wagner, Platelet activation, aggregation, and life span in calves implanted with axial flow ventricular assist devices, *Ann. Thorac. Surg*. **73** (2002), 1933–1938.
[25] E.N. Sorensen, G.W. Burgreen, W.R. Wagner and J.F. Antaki, Computational simulation of platelet deposition and activation: I. Model development and properties, *Ann. Biomed. Eng*. **27** (1999), 436–448.
[26] A.W. Tilles and E.C. Eckstein, The near-wall excess of platelet-sized particles in blood flow: its dependence on hematocrit and wall shear rate, *Microvasc. Res*. **33** (1987), 211–223.
[27] H.F. van Breugel, P.G. de Groot, R.M. Heethaar and J.J. Sixma, Role of plasma viscosity in platelet adhesion, *Blood* **80** (1992), 953–959.
[28] F.M. White, *Viscous Fluid Flow*, McGaw-Hill, Inc., New York, 1991, 736 pp.
[29] C. Xu and D.M. Wootton, Platelet near-wall excess in porcine whole blood in artery-sized tubes under steady and pulsatile flow conditions, *Biorheology* **41** (2004), 113–125.
[30] H. Yamanaka, G. Rosenberg, W.J. Weiss, A.J. Snyder, C.M. Zapanta and C.A. Siedlecki, Multiscale analysis of surface thrombosis in vivo in a left ventricular assist system, *ASAIO J*. **51** (2005), 567–577.
[31] H. Yamanaka, G. Rosenberg, W.J. Weiss, A.J. Snyder, C.M. Zapanta and C.A. Siedlecki, Short-term in vivo studies of surface thrombosis in a left ventricular assist system, *ASAIO J*. **52** (2006), 257–265.
[32] R. Zhao, J.F. Antaki, T. Naik, T.N. Bachman, M.V. Kameneva and Z.J. Wu, Microscopic investigation of erythrocyte deformation dynamics, *Biorheology* **43** (2006), 747–765.